Impurity effect and vortex cluster phase in mesoscopic type-1.5 superconductors

Guo Wang[1], Tian-Yi Han[1], Jie Li[1] and Hai Huang[2⋆]

1 School of Nuclear Science and Engineering, North China Electric Power University, Beijing, 102206, P. R. China

2 Department of Mathematics and Physics, North China Electric Power University, Beijing, 102206, P. R. China

⋆ huanghai@ncepu.edu.cn

Abstract

Based on two-band time-dependent Ginzburg-Landau theory, we study the electromagnetic properties of mesoscopic type-1.5 superconductors with different defect configurations. We perform the numerical simulations with the finite element method, and give the direct evidence for the existence of vortex cluster phase in the presence of nonmagnetic impurities. In addition, we also investigate the effects of impurity number and anisotropic defect structure on the patterns of magnetic vortex distributions. Our theoretical results thus indicate that the diversity of impurity deposition has a significant influence on the semi-Meissner state in type-1.5 superconductors.

Publication information to appear upon publication.

Received Date
Accepted Date
Published Date

Contents

---

1 Introduction

Over the past two decades, two-band superconductivity has become an important research subject in condensed matter physics. This field started from the discovery of superconductivity in MgB_2 [1], where the existence of two distinct superconducting gaps reveals the complexity of Fermi surface topology in this system. Since then, extensive theoretical and experimental studies have been performed to provide novel insights into unconventional superconducting pairing mechanisms and physical properties in these materials. For example, the multi-gap superconductivity signals a new pathway to achieve more superconducting pairing modes, which can induce phase competition or coexistence between multiple bands by adjusting the external magnetic field or impurity distribution. Furthermore, the magnetic vortex behavior can be optimized through rational design of multi-band structures and its interaction with impurities can improve the overall performance of superconducting devices [2,3].

As we know, each condensate in two-band superconductors is predicted to support vortex excitation with fractional quantum flux [4,5]. Due to the interband Josephson coupling, the vortices from different condensates are bounded together with the string interaction and their normal cores will be locked to form a composite vortex with the standard integer quantum flux. Therefore, the vortex physics in two-band systems is influenced by the coherence lengths ξ_1 and ξ_2 as well as the magnetic field penetration depth λ. When the particular condition $\xi_1 < \sqrt{2}\lambda < \xi_2$ is satisfied, there may exhibit a new superconducting state that combines characteristics of both type-1 and type-2 superconductors. This so-called semi-Meissner phase or vortex cluster phase is formed due to the interaction of long-range attraction and short-range repulsion between composite vortex excitations [6–8]. The existence of this novel vortex pattern was first visualized by Bitter decorations on high quality MgB_2 single crystal in 2009 [9]. Thereafter, zero-field muon spin experiments have also revealed the presence of this type-1.5 superconducting state in unconventional superconductors Sr_2RuO_4 [10,11] and $LaPt_3Si$ [12,13].

In the present paper, we study the electromagnetic effect of mesoscopic type-1.5 superconductors with different impurity distributions based on the time-dependent Ginzburg-Landau (TDGL) theory. With the COMSOL Multiphysics software and the finite element method, our results directly show the crossover of this mesoscopic system from the diamagnetic Meissner state to the vortex cluster phase, and ultimately to the Abrikosov lattice phase. We also observe that with the increase of isotropic defect number, multiple vortex clusters will be generated around the pinning centers and each cluster exhibits the identical configuration with hexagonal symmetry. Furthermore, we discuss the possible pattern of vortex cluster induced by an anisotropic impurity in this superconductor. All of our theoretical results indicate that the diversity of impurity deposition has a significant influence on the collective behaviors of magnetic vortices in the type-1.5 superconducting system.

The rest of this article is organized as follows. In Sec. 2, we introduce the two-band TDGL theory and apply this formalism to the type-1.5 superconductors. In Sec. 3, we give the procedure of numerical simulations based on the finite element method. Then in Sec. 4, we discuss the impurity effect and vortex cluster phase in the mesoscopic system. Finally, Sec. 5 gives the conclusion of the paper.

2 Model and formalism

The simplest GL free energy functional of two-gap superconductors can be written as [14–18]

$$F = \sum_i \left[\frac{1}{2m_i} \left| \left(-i\hbar\boldsymbol{\nabla} - \frac{2e}{c}\boldsymbol{A} \right) \Psi_i \right|^2 - \alpha_i |\Psi_i|^2 + \frac{\beta_i}{2} |\Psi_i|^4 \right] + \frac{\boldsymbol{B}^2}{8\pi}. \tag{1}$$

Here Ψ_i $(i = 1,2)$ represents the superconducting order parameter and m_i is the effective mass for each band. The coefficient α_i is a function of temperature, while β_i is independent of temperature. In the presence of impurities, the parameters α_1 and α_2 can be approximately expressed as $\alpha_i = \alpha_{i0} f(\boldsymbol{r})$. Here we introduce a function $f(\boldsymbol{r})$ between -1 and $+1$ to model the defect sites which will deplete the superconducting state at specific positions [19, 20]. $\boldsymbol{B} = \boldsymbol{\nabla} \times \boldsymbol{A}$ is the magnetic field and $\boldsymbol{A}$ is the vector potential.

If the superconductor is driven out of equilibrium, the order parameter should relax back to its equilibrium value. It is well known that this deviation of superconducting materials can be conveniently described by the TDGL theories. The single-band TDGL equations were first proposed by Schmid [21] and derived from the microscopic BCS theory by Gor'kov and Éliashberg [22]. The extension of TDGL equations to the multi-component superconducting system can be written as [23–25]

$$-\Gamma_i \frac{\partial \Psi_i}{\partial t} = \frac{\delta F}{\delta \Psi_i^*} \quad \text{and} \quad -\sigma_n \frac{\partial \boldsymbol{A}}{\partial t} = \frac{\delta F}{\delta \boldsymbol{A}} \tag{2}$$

where Γ_i is the relaxation time of order parameters and σ_n represents the electrical conductivity of the normal sample in the two-band case. Therefore, minimization of the free energy F with respect to Ψ_i and $\boldsymbol{A}$ leads to the following dimensionless TDGL equations in the zero-electrostatic potential gauge

$$-\Gamma_1 \frac{\partial \Psi_1}{\partial t} = (-\mathrm{i}\boldsymbol{\nabla} - \boldsymbol{A})^2 \Psi_1 - \left[f(\boldsymbol{r}) - \left|\Psi_1\right|^2 \right] \Psi_1, \tag{3}$$

$$-\Gamma_2 \frac{\partial \Psi_2}{\partial t} = \frac{m_1}{m_2} (-\mathrm{i}\boldsymbol{\nabla} - \boldsymbol{A})^2 \Psi_2 - \left[\frac{\alpha_{20}}{\alpha_{10}} f(\boldsymbol{r}) - \frac{\beta_2}{\beta_1} \left|\Psi_2\right|^2 \right] \Psi_2 \tag{4}$$

and

$$-\frac{\partial \boldsymbol{A}}{\partial t} = \kappa_1^2 \boldsymbol{\nabla} \times \boldsymbol{\nabla} \times \boldsymbol{A} - \boldsymbol{J}_s \tag{5}$$

with the supercurrent

$$\boldsymbol{J}_s = \frac{\mathrm{i}}{2} \left(\Psi_1 \boldsymbol{\nabla} \Psi_1^* - \Psi_1^* \boldsymbol{\nabla} \Psi_1 \right) - \left|\Psi_1\right|^2 \boldsymbol{A} + \frac{m_1}{m_2} \left[\frac{\mathrm{i}}{2} \left(\Psi_2 \boldsymbol{\nabla} \Psi_2^* - \Psi_2^* \boldsymbol{\nabla} \Psi_2 \right) - \left|\Psi_2\right|^2 \boldsymbol{A} \right]. \tag{6}$$

Here in the clean limit with the impurity function $f = 1$, we at first introduce the coherence length $\xi_i^2 = \hbar^2/(2m_i\alpha_{i0})$, the London penetration depth $\lambda^{-2} = \lambda_1^{-2} + \lambda_2^{-2}$ with $\lambda_i^{-2} = 4\pi e^2 \Psi_{i0}^2/(m_i c^2)$ and $\Psi_{i0} = \sqrt{\alpha_{i0}/\beta_i}$, and the GL parameter $\kappa_1 = \lambda_1/\xi_1$. We then take the coordinate $\boldsymbol{r}$ in units of ξ_1, the time t in units of $t_0 = m_1\sigma_n/\left(4e^2\Psi_{10}^2\right)$, Γ_i in units of $\alpha_{10} t_0$ and the order parameter Ψ_i in units of Ψ_{10}. We also set the magnetic field $\boldsymbol{B}$ in units of $H_0 = \Phi_0/\left(2\pi\xi_1^2\right)$ with the flux quantum $\Phi_0 = \pi\hbar c/e$ and the vector potential $\boldsymbol{A}$ in units of $A_0 = H_0 \xi_1$.

Following Ref. [6], multi-component systems allow a type of superconductivity that is distinct from type-1 or type-2 superconductor. With the condition $\xi_1 < \sqrt{2}\lambda < \xi_2$, the type-1.5 superconducting state will originate from a peculiar vortex interaction which exhibits short-range repulsion and long-range attraction characteristics. The short-range repulsion prevents adjacent vortices from overlapping, while the long-range attraction facilitates the clustering of composite vortices. Consequently, this state is different from type-1 superconductors that completely repel magnetic flux and type-2 superconductors which allow considerable magnetic flux penetration and the formation of vortex lattice. In the ideal sample, the constraint mentioned above can be specifically expressed as

$$\sqrt{\frac{1}{2}\left(1 + \frac{m_1}{m_2}\frac{\alpha_{20}}{\alpha_{10}}\frac{\beta_1}{\beta_2}\right)} < \kappa_1 < \sqrt{\frac{1}{2}\left[\frac{m_1}{m_2}\frac{\alpha_{10}}{\alpha_{20}} + \left(\frac{m_1}{m_2}\right)^2 \frac{\beta_1}{\beta_2}\right]}. \tag{7}$$

In this circumstance, the magnetic composite vortices will form vortex clusters and coexist with domains of the two-component Meissner state in the framework of the GL theory.

In order to numerically solve Eqs. (3)-(5), we need to specify appropriate boundary conditions of the superconducting sample. We use the following superconductor-insulator (or vacuum) boundary conditions [26–28]

$$\nabla\Psi_i \cdot \boldsymbol{n} = 0, \quad \boldsymbol{A}\cdot\boldsymbol{n} = 0 \quad \text{and} \quad \nabla\times\boldsymbol{A} = \boldsymbol{H}_e \tag{8}$$

where $\boldsymbol{n}$ is the outward unit vector normal to the boundary and the external applied magnetic field is set as $\boldsymbol{H}_e = H_e\hat{\boldsymbol{z}}$. The first two conditions just indicate that any current passing through the interface between a superconducting domain and vacuum/insulator would be nonphysical. The third equation represents the continuity of magnetic field across the boundary. The partial differential equations (3)-(5) will be solved numerically for the mesoscopic geometry in the two-dimensional space. The initial conditions at $t = 0$ are taken as $|\Psi_i| = 1$ and $\boldsymbol{A} = (0,0)$ on the xy-plane, corresponding to the Meissner state and zero magnetic field inside the superconductor.

3 Finite element method and numerical computations

Based on the COMSOL Multiphysics software platform [29], we will describe the procedure of the numerical simulations on the TDGL equations in this section. We first split the order parameters into the real and imaginary parts, i.e. $\Psi_1 = u_1 + iu_2$ and $\Psi_2 = u_3 + iu_4$. The magnetic potential is also written in component form as $\boldsymbol{A} = (u_5, u_6)$. In order to implement the boundary conditions, we will introduce an auxiliary variable $u_7(x, y, t)$ for reasons explained below. In the procedure of simulations, we set $\Gamma_1 = \Gamma_2 = 5$ and $m_1 = 2m_2$. To stabilize the semi-Meissner state, we also take $\alpha_{10} = \alpha_{20}$ and $\beta_1 = \beta_2$ in the calculations.

In this way, we can transform the TDGL equations into the general form of partial differential equations in this software package

$$\sum_k \mu_{jk}\frac{\partial u_k}{\partial t} + \sum_l \partial_l \nu_{jl} = \eta_j. \tag{9}$$

Here we have $j, k = 1, 2, \cdots, 7$, $l = 1, 2$ and $(\partial_1, \partial_2) = (\partial_x, \partial_y)$. The 7×7 matrix μ_{jk} and the 7×2 column vector ν_{jl} take the form

$$\mu_{jk} = \begin{bmatrix} 5 & 0 & 0 & 0 & 0 & 0 & 0 \\ 0 & 5 & 0 & 0 & 0 & 0 & 0 \\ 0 & 0 & 5 & 0 & 0 & 0 & 0 \\ 0 & 0 & 0 & 5 & 0 & 0 & 0 \\ 0 & 0 & 0 & 0 & 1 & 0 & 0 \\ 0 & 0 & 0 & 0 & 0 & 1 & 0 \\ 0 & 0 & 0 & 0 & 0 & 0 & 0 \end{bmatrix} \tag{10}$$

and

$$\nu_{jl} = \begin{bmatrix} -u_{1x} & -u_{1y} \\ -u_{2x} & -u_{2y} \\ -2u_{3x} & -2u_{3y} \\ -2u_{4x} & -2u_{4y} \\ 0 & \kappa_1^2\left(u_{6x} - u_{5y} - H_e\right) \\ \kappa_1^2\left(u_{5y} - u_{6x} + H_e\right) & 0 \\ u_5 & u_6 \end{bmatrix}. \tag{11}$$

Noting that the subscript x or y denotes the partial derivative with respect to the corresponding variable here. Meanwhile, the driving force η_j contains all other terms in the TDGL equations except the left handed side of Eq. (9), and detailed calculations will give all the components explicitly as

$$\eta_1 = \left[f(\boldsymbol{r}) - \left(u_1^2 + u_2^2 + u_5^2 + u_6^2\right)\right] u_1 + \left(u_{5x} + u_{6y}\right) u_2 + 2\left(u_{2x}u_5 + u_{2y}u_6\right), \tag{12}$$

$$\eta_2 = \left[f(\boldsymbol{r}) - \left(u_1^2 + u_2^2 + u_5^2 + u_6^2\right)\right] u_2 - \left(u_{5x} + u_{6y}\right) u_1 - 2\left(u_{1x}u_5 + u_{1y}u_6\right), \tag{13}$$

$$\eta_3 = \left[f(\boldsymbol{r}) - \left(u_3^2 + u_4^2\right) - 2\left(u_5^2 + u_6^2\right)\right] u_3 + 2\left(u_{5x} + u_{6y}\right) u_4 + 4\left(u_{4x}u_5 + u_{4y}u_6\right), \tag{14}$$

$$\eta_4 = \left[f(\boldsymbol{r}) - \left(u_3^2 + u_4^2\right) - 2\left(u_5^2 + u_6^2\right)\right] u_4 - 2\left(u_{5x} + u_{6y}\right) u_3 - 4\left(u_{3x}u_5 + u_{3y}u_6\right), \tag{15}$$

$$\eta_5 = \left(u_{2x}u_1 - u_{1x}u_2\right) - \left(u_1^2 + u_2^2\right) u_5 + 2\left[\left(u_{4x}u_3 - u_{3x}u_4\right) - \left(u_3^2 + u_4^2\right) u_5\right], \tag{16}$$

$$\eta_6 = \left(u_{2y}u_1 - u_{1y}u_2\right) - \left(u_1^2 + u_2^2\right) u_6 + 2\left[\left(u_{4y}u_3 - u_{3y}u_4\right) - \left(u_3^2 + u_4^2\right) u_6\right], \tag{17}$$

$$\eta_7 = u_{5x} + u_{6y} + u_7. \tag{18}$$

Now we can examine the boundary conditions in this formalism. With the normal vector $\boldsymbol{n} = (n_1, n_2)$ and the column vector ν_{jl}, the boundary conditions in Eq. (8) can be simply casted into the compact form as

$$\sum_l n_l \nu_{jl} = 0 \tag{19}$$

which is best suited to the COMSOL Multiphysics simulations. We also note that from the last equation ($j = 7$) in (9), our manipulations will give a trivial solution $u_7 = 0$ for this auxiliary variable and it insures the self-consistency of our problem.

COMSOL Multiphysics is a versatile and advanced simulation platform which is designed to tackle complex engineering and scientific problems. Its core principle is to numerically solve partial differential equations based on finite element method [30–32]. The process begins with discretizing the computational domain and subdividing the lattice cell into small subregions called elements. Triangular elements are preferred due to their flexibility in handling complex and irregular shapes. It will transform the continuous domain into a finite element mesh and enable precise numerical computations. Following this step, a function space typically composed of piecewise continuous polynomials is constructed to ensure smoothness across element boundaries. Subsequently, Lagrangian shape functions are selected as basis functions for their ability to achieve high computational accuracy and numerical stability [33]. Finally, the software employs an implicit solver that typically incorporates consistent initialization of the backward Euler method to ensure significant stability for time-dependent simulations. In our numerical computations, we take the time step $\Delta t = 0.5 t_0$ and the relative tolerance 10^{-8} to control the convergence of the transient calculations for our system.

4 Results and discussions

In this section, we will set the external magnetic field to $H_e = 0.8 H_0$ and discuss the effect of impurity on the patterns of magnetic vortex distribution in the $15\xi_1 \times 15\xi_1$ type-1.5 superconductor. Following Refs. [19] and [20], we have chosen the impurity function f to take the phenomenological form

$$f(\boldsymbol{r}) = \prod_{n=1}^{N} f_n(\boldsymbol{r}) \text{ with } f_n(\boldsymbol{r}) = \begin{cases} -0.5, \text{ if } |\boldsymbol{r} - \boldsymbol{r}_{0n}| < R \left|\cos\left[p\left(\theta + \pi/4\right)\right]\right| \\ 1\,, \qquad \text{otherwise} \end{cases} . \tag{20}$$

It is easy to see that the shape of impurities centered at $\boldsymbol{r}_{0n} = (x_{0n}, y_{0n})$ with $n = 1, 2, ..., N$, depends on the angle θ and different integer values of p. This means that the defect sites can be isotropic with radius R when $p = 0$ and anisotropic with $2p$-fold symmetry at $p \neq 0$. We take $R = 0.5\xi_1$ for each pinning state in the simulations.

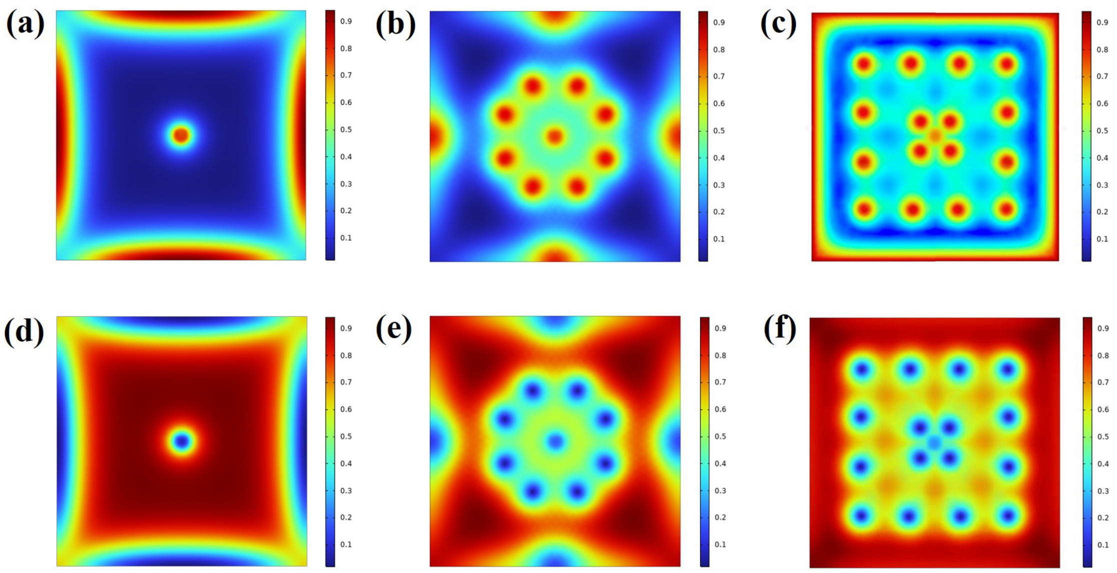

Figure 1: Evolution of the magnetic flux density B_z (a-c) and the order parameter of the first condensate $|\Psi_1|$ (d-f) at the presence of an isotropic defect in the $15\xi_1 \times 15\xi_1$ type-1.5 superconductor. The snapshots show the Meissner phase (a,d), vortex cluster phase (b,e) and vortex lattice phase (c,f) at the GL parameter $\kappa_1 = 0.70$, 1.30 and 2.10 respectively. The magnetization only has the component perpendicular to the superconducting plane.

To verify the availability of the method, we first take the impurity function with $N = 1$, $p = 0$ and insert this pinning site at the center of the superconducting square. We then plot the magnetic flux density $B_z = u_{6x} - u_{5y}$ in units of H_0 (a-c) and the order parameter of the first condensate $|\Psi_1| = \sqrt{u_1^2 + u_2^2}$ in units of Ψ_{10} (d-f) at $t = 10^4 t_0$ in Fig. 1. With the GL parameter κ_1 taken as 0.70, 1.30 and 2.10 sequentially, we can clearly observe the crossover of this type-1.5 system from the perfect diamagnetism state to the vortex cluster

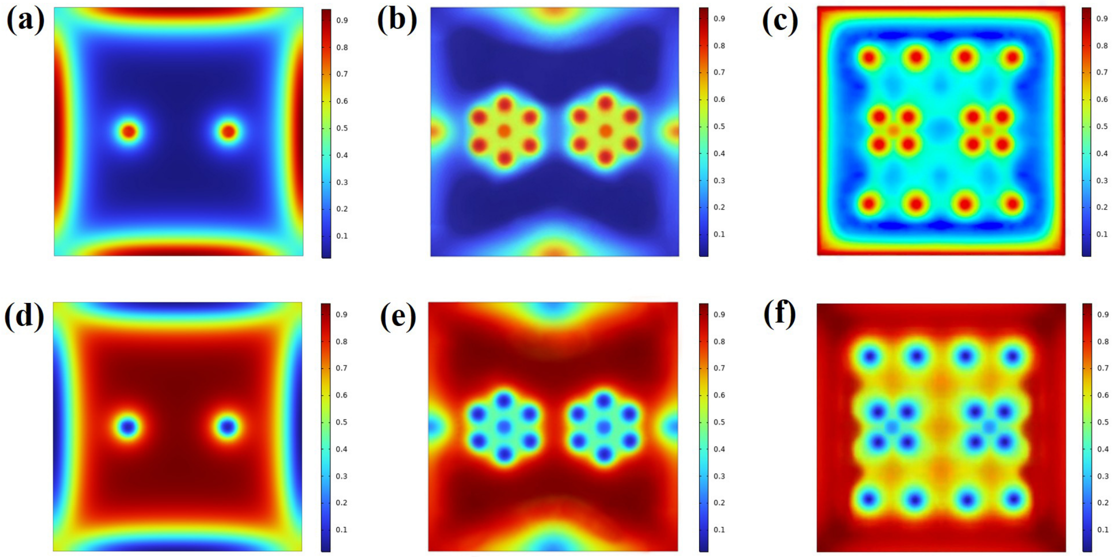

Figure 2: Evolution of the magnetic flux density B_z (a-c) and the order parameter of the first condensate $|\Psi_1|$ (d-f) at the presence of two isotropic defects in the $15\xi_1 \times 15\xi_1$ type-1.5 superconductor. The snapshots show the Meissner phase (a,d), multiple cluster phase (b,e) and vortex lattice phase (c,f) at the GL parameter $\kappa_1 = 0.70$, 1.30 and 2.10 respectively. The magnetization only has the component perpendicular to the superconducting plane.

phase, and ultimately to the Abrikosov vortex lattice. Our numerical simulations also show that the cluster phase presents the vortex pattern with octagonal symmetry and appears in the region of $1.08 < \kappa_1 < 1.58$. Meanwhile, from Eq. (7) we expect to discover the semi-Meissner state within $1.22 < \kappa_1 < 1.73$ in the clean limit. According to Ref. [34], the introduction of impurity into the material will enhance the effective magnetic penetration depth, thus leading to a larger effective GL parameter. Therefore, this allows the magnetic vortex phases to be observed at smaller κ_1 values in type-1.5 superconductors. Moreover, it is easy to see that the isotropic defect induces the localized distortions of the flux lattice without breaking the C_4 rotational symmetry of the superconducting square.

Furthermore, we also perform the simulations on time evolution of the mesoscopic type-1.5 superconductor with multiple isotropic defects. For $N = 2$ and $p = 0$, we select the pinning centers at $(\pm 3\xi_1, 0)$ and plot the B_z and $|\Psi_1|$ at $t = 10^4 t_0$ in Fig. 2. Different from the single impurity case, multiple vortex clusters are generated around the pinning sites within $0.87 < \kappa_1 < 1.40$. With the GL parameter $\kappa_1 = 1.30$, we can see from Fig. 2(b,e) that each vortex cluster exhibits the identical pattern with hexagonal symmetry. Meanwhile for $\kappa_1 = 2.10$, as shown in Fig. 2(c,f), we can clearly observe multiple localized distortions in the flux lattice around the pinning positions due to the attraction of vortices by impurities.

Besides that, we perform the simulations on this mesoscopic type-1.5 system with an anisotropic defect. For $N = 1$ and $p = 2$, we still take the impurity site at the center of the superconducting square and plot the B_z and $|\Psi_1|$ at $t = 10^4 t_0$ in Fig. 3. By setting κ_1 as 1.30 and 2.10, we can observe the novel vortex cluster with C_4 (not C_8 in isotropic impurity case) symmetry shown in Fig. 3(b,e) and the distorted flux lattice in Fig. 3(c,f) respectively. Our numerical data also indicate that the vortex cluster phase exists in the regime $1.15 < \kappa_1 < 1.67$ for this mesoscopic superconductor. As we see the anisotropic defect occupies the smaller normal area compared with its isotropic counterpart, this will lead to the greater κ_1 for the emergence of the magnetic vortex phases.

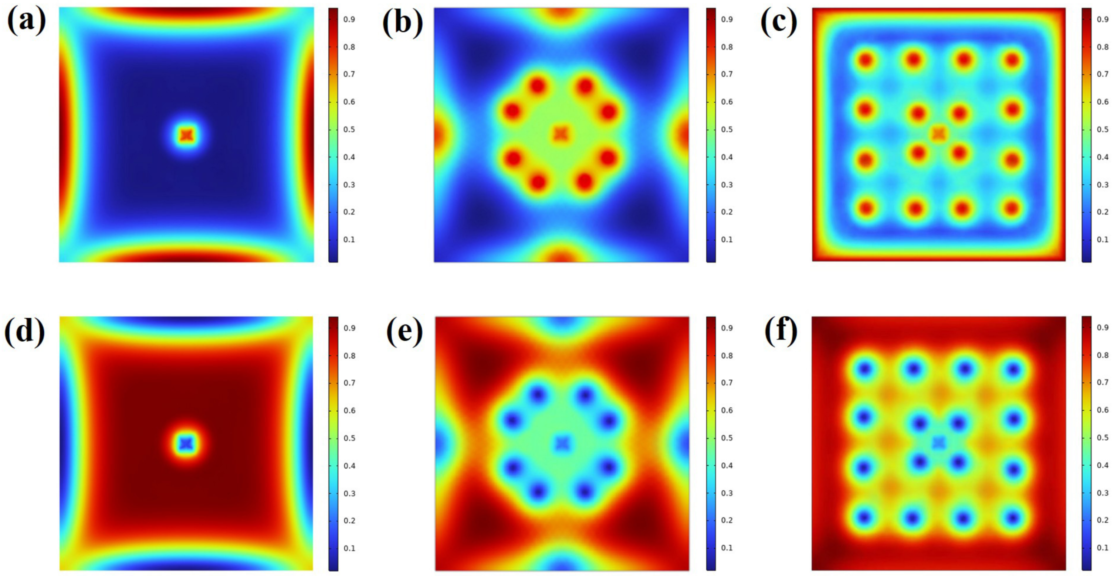

Figure 3: Evolution of the magnetic flux density B_z (a-c) and the order parameter of the first condensate $|\Psi_1|$ (d-f) at the presence of an anisotropic defect in the $15\xi_1 \times 15\xi_1$ type-1.5 superconductor. The snapshots show the Meissner phase (a,d), vortex cluster phase (b,e) and vortex lattice phase (c,f) at the GL parameter $\kappa_1 = 0.70$, 1.30 and 2.10 respectively. The magnetization only has the component perpendicular to the superconducting plane.

5 Conclusion

Based on two-band TDGL theory, we investigate the impurity effect on the vortex collective behaviors in the mesoscopic type-1.5 superconductor. With the finite element method, our numerical results give the direct evidence for the existence of vortex cluster phase at the presence of nonmagnetic defects in this system. We also discuss the possible patterns of vortex cluster state with multiple impurities and anisotropic defect structure. We hope that our theoretical results will inspire further research on better understanding novel vortex dynamics and transport properties in two-band superconductors.

Author contributions Conceptualization, G.W., T.H., J.L. and H.H.; methodology, G.W., T.H., J.L. and H.H.; software, G.W.; validation, T.H., J.L. and H.H.; formal analysis, G.W., T.H., J.L. and H.H.; investigation, G.W., T.H., J.L. and H.H.; resources, H.H.; data curation, G.W.,T.H., J.L. and H.H.; writing-original draft preparation, G.W.,T.H. and H.H.; writing-review and editing, G.W., T.H., J.L. and H.H.; visualization, G.W.; supervision, T.H., J.L. and H.H.; project administration, H.H. All authors have read and agreed to the published version of the manuscript.

References

[1] J. Nagamatsu, N. Nakagawa, T. Muranaka, Y. Zenitani and J. Akimitsu, *Superconductivity at 39 K in magnesium diboride*, Nature **410**, 63 (2001), doi:10.1038/35065039.

[2] M. Zehetmayer, *A review of two-band superconductivity: materials and effects on the thermodynamic and reversible mixed-state properties*, Supercond. Sci. Technol. **26**, 043001

(2013), doi:10.1088/0953-2048/26/4/043001.

[3] T. Salamone, H. G. Hugdal, S. H. Jacobsen and Morten Amundsen, *High magnetic field superconductivity in a two-band superconductor*, Phys. Rev. B **107**, 174516 (2023), doi:10.1103/PhysRevB.107.174516.

[4] Y. Tanaka, *Soliton in two-band superconductor*, Phys. Rev. Lett. **88**, 017002 (2002), doi:10.1103/PhysRevLett.88.017002.

[5] E. Babaev, *Vortices with fractional flux in two-gap superconductors and in extended Faddeev model*, Phys. Rev. Lett. **89**, 067001 (2002), doi:10.1103/PhysRevLett.89.067001.

[6] E. Babaev and M. Speight, *Semi-Meissner state and neither type-I nor type-II superconductivity in multicomponent superconductors*, Phys. Rev. B **72**, 180502 (2005), doi:10.1103/PhysRevB.72.180502.

[7] J. Carlström, E. Babaev and M. Speight, *Type-1.5 superconductivity in multiband systems: effects of interband couplings*, Phys. Rev. B **83**, 174509 (2011), doi:10.1103/PhysRevB.83.174509.

[8] J. Carlström, J. Garaud and E. Babaev, *Length scales, collective modes, and type-1.5 regimes in three-band superconductors*, Phys. Rev. B **84**, 134518 (2011), doi:10.1103/PhysRevB.84.134518.

[9] V. Moshchalkov, M. Menghini, T. Nishio, Q. H. Chen, A. V. Silhanek, V. H. Dao, L. F. Chibotaru, N. D. Zhigadlo and J. Karpinski, *Type-1.5 superconductivity*, Phys. Rev. Lett. **102**, 117001 (2009), doi:10.1103/PhysRevLett.102.117001.

[10] C. W. Hicks, J. R. Kirtley, T. M. Lippman, N. C. Koshnick, M. E. Huber, Y. Maeno, W. M. Yuhasz, M. B. Maple and K. A. Moler, *Limits on superconductivity-related magnetization in Sr_2RuO_4 and $PrOs_4Sb_{12}$ from scanning SQUID microscopy*, Phys. Rev. B **81**, 214501 (2010), doi:10.1103/PhysRevB.81.214501.

[11] S. J. Ray, A. S. Gibbs, S. J. Bending, P. J. Curran, E. Babaev, C. Baines, A. P. Mackenzie and S. L. Lee, *Muon-spin rotation measurements of the vortex state in Sr_2RuO_4: type-1.5 superconductivity, vortex clustering, and a crossover from a triangular to a square vortex lattice*, Phys. Rev. B **89**, 094504 (2014), doi:10.1103/PhysRevB.89.094504.

[12] I. Kawasaki, I. Watanabe, H. Amitsuka, K. Kunimori, H. Tanida and Y. Onuki, *Superconducting properties of noncentrosymmetric superconductor $LaPt_3Si$ studied by muon spin spectroscopy*, J. Phys. Soc. Jpn. **82**, 084713 (2013), doi:10.7566/JPSJ.82.084713.

[13] T. Fujisawa, A. Yamaguchi, G. Motoyama, D. Kawakatsu, A. Sumiyama, T. Takeuchi, R. Settai and Y. Onuki, *Magnetization measurements of non-centrosymmetric superconductor $LaPt_3Si$: construction of low temperature magnetometers with the SQUID and Hall sensor*, Jpn. J. Appl. Phys. **54**, 048001 (2015), doi:10.7567/JJAP.54.048001.

[14] Y. S. Yerin and A. N. Omelyanchouk, *Coherent current states in a two-band superconductor*, Low Temp. Phys. **33**, 401 (2007), doi:10.1063/1.2737547.

[15] R. M. Silva, M. V. Milošević, D. Domínguez, F. M. Peeters and J. A. Aguiar, *Distinct magnetic signatures of fractional vortex configurations in multiband superconductors*, Appl. Phys. Lett. **105**, 232601 (2014), doi:10.1063/1.4904010.

[16] S. Maiti, M. Sigrist and A. Chubukov, *Spontaneous currents in a superconductor with $s+is$ symmetry*, Phys. Rev. B **91**, 161102 (2015), doi:10.1103/PhysRevB.91.161102.

[17] J. Garaud, M. Silaev and E. Babaev, *Thermoelectric signatures of time-reversal symmetry breaking states in multiband superconductors*, Phys. Rev. Lett. **116**, 097002 (2016), doi:10.1103/PhysRevLett.116.097002.

[18] V. L. Vadimov and M. A. Silaev, *Polarization of the spontaneous magnetic field and magnetic fluctuations in $s+is$ anisotropic multiband superconductors*, Phys. Rev. B **98**, 104504 (2018), doi:10.1103/PhysRevB.98.104504.

[19] S. Z. Lin, S. Maiti and A. Chubukov, *Distinguishing between $s+id$ and $s+is$ pairing symmetries in multiband superconductors through spontaneous magnetization pattern induced by a defect*, Phys. Rev. B **94**, 064519 (2016), doi:10.1103/PhysRevB.94.064519.

[20] M. P. Srensen, N. F. Pedersenand and M. Ögren, *The dynamics of magnetic vortices in type II superconductors with pinning sites studied by the time dependent Ginzburg-Landau model*, Physica C **533**, 40 (2017), doi:10.1016/j.physc.2016.08.001.

[21] A. Schmid, *A time dependent Ginzburg-Landau equation and its application to the problem of resistivity in the mixed state*, Phys. Kondens. Mater. **5**, 302 (1966), doi:10.1007/BF02422669.

[22] L. P. Gor'kov and G. M. Éliashberg, *Generlization of the Ginzburg-Landau equations for non-stationaryproblems in the case of alloys with paramagnetic impurities*, Zh. Eksp. Teor. Fiz. **54**, 612 (1968), doi:10.1142/9789814317344_0003.

[23] P. A. S. Mosquera, R. M. da Silva, A. Vagov, A. A. Shanenko, T. C. E. Deluque and A. J. Albino, *Nonequilibrium interband phase textures induced by vortex splitting in two-band superconductors*, Phys. Rev. B **96**, 054517 (2017), doi:10.1103/PhysRevB.96.054517.

[24] C. A. Aguirre, M. R. Joya and J. Barba-Ortega, *On the vortex matter in a two-band superconducting meso-prism*, Physica C **585**, 1353867 (2021), doi:10.1016/j.physc.2021.1353867.

[25] S. Z. Du, Y. N. Zhong, S. W. Yao, L. Peng, T. T. Shi, L. N. Sang, X. L. Liu and J. Lin, *The dynamics of current-driven vortex in two-band superconductor with $s+d$ wave pairing*, Phys. Lett. A **443**, 128206 (2022), doi:10.1016/j.physleta.2022.128206.

[26] S. W. Yao, L. Peng, J. Lin, J. Chen, C. B. Cai and Y. Zhou, *Properties of vortex configurations in two-band mesoscopic superconductors with Josphson coupling: the Ginzburg-Landau theory*, J. Low. Temp. Phys. **202**, 329 (2021), doi:10.1007/s10909-020-02551-x.

[27] Y. G. Ryu, G. I. Mun, Y. N. Kwon, S. H. Kim and S. Hong, *Motion of magnetic vortices in type-II superconductor with randomly distributed pinning centers*, Physica C **602**, 1354125 (2022), doi:10.1016/j.physc.2022.1354125.

[28] Y. G. Ryu, J. H. Om, J. H. Kim, G. I. Ro, G. I. Mun and S. Hong, *The influence of surface defects on motion of magnetic vortices in mesoscopic type-II superconductor with randomly distributed pinning centers*, J. Supercond. Nov. Magn. **37**, 527 (2024), doi:10.1007/s10948-024-06694-w.

[29] COMSOL, Comsol multiphysics modeling guide, (2009), https://www.comsol.com.

[30] Q. Du, M. D. Gunzburger and J. S. Peterson, *Solving the Ginzburg-Landau equations by finite-element methods*, Phys. Rev. B **46**, 9027 (1992), doi:10.1103/PhysRevB.46.9027.

[31] T. S. Alstrm, M. P. Srensen, N. F. Pedersen and S. Madsen, *Magnetic flux lines in complex geometry type-II superconductors studied by the time dependent Ginzburg-Landau equation*, Acta. Appl. Math. **115**, 63 (2011), doi:10.1007/s10440-010-9580-8.

[32] B. Oripov and S. M. Anlage, *Time-dependent Ginzburg-Landau treatment of rf magnetic vortices in superconductors: vortex semiloops in a spatially nonuniform magnetic field*, Phys. Rev. E **101**, 033306 (2020), doi:10.1103/PhysRevE.101.033306.

[33] J. C. Li and Y. Q. Huang, *Time-domain finite element methods for Maxwell's equations in metamaterials*, Springer Heidelberg, New York, Dordrecht London, ISBN 978-3-642-33788-8 (2013), doi:10.1007/978-3-642-33789-5.

[34] M. Tinkham, *Introduction to superconductivity*, McGraw-Hill, New York, USA, ISBN 0-07-064878-6 (1996), doi:10.1063/1.2807811.